Cell Reports
Physical Science

CellPress
OPEN ACCESS

Article

Harnessing precursor-directed biosynthesis with glucose derivatives to access cotton fibers with enhanced physical properties

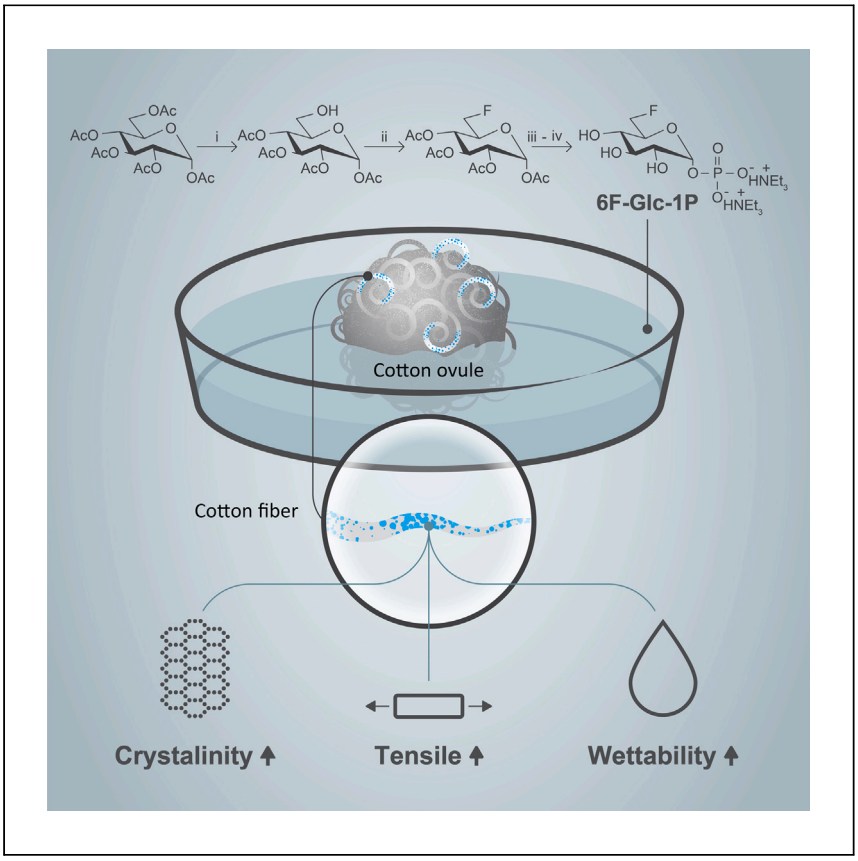

A chemically synthesized glucosyl phosphate derivative is fed to *in vitro*-growing cotton ovules, resulting in derivative incorporation into the fibers while bypassing the initial steps in glucose metabolism. Aharon Kuperman et al. show this process alters cellulose structure and enhances crystallinity, improving mechanical and water adsorption properties of cotton fibers.

Ofir Aharon Kuperman, Peterson de Andrade, XiaoMeng Sui, ..., Jacob Judas Kain Kirkensgaard, Robert A. Field, Filipe Natalio

filipe.natalio@weizmann.ac.il

Highlights

Glucosyl phosphate derivative 6F-Glc-1P is synthesized and fed to fertilized cotton ovules

6F-Glc and fluorine ions are identified on and within the resulting fibers

Treated fibers exhibit altered crystalline structure and increased crystallinity

Fiber modification results in enhanced mechanical properties and wettability

Kuperman et al., Cell Reports Physical Science 5, 101963
May 15, 2024
https://doi.org/10.1016/j.xcrp.2024.101963

Cell Reports
Physical Science

CellPress
OPEN ACCESS

Article

Harnessing precursor-directed biosynthesis with glucose derivatives to access cotton fibers with enhanced physical properties

Ofir Aharon Kuperman,[1,10] Peterson de Andrade,[2,10] XiaoMeng Sui,[3] Raquel Maria,[4] Ifat Kaplan-Ashiri,[3] Qixiang Jiang,[5] Tanguy Terlier,[6] Jacob Judas Kain Kirkensgaard,[7,8] Robert A. Field,[2,9] and Filipe Natalio[1,11,*]

SUMMARY

Cotton ovule *in vitro* cultures are a promising platform for exploring biofabrication of fibers with tailored properties. When the ovules' growth medium is supplemented with chemically synthesized cellulose precursors, it results in their integration into the developing fibers, thereby tailoring their end properties. Here, we report the feeding of synthetic glucosyl phosphate derivative, 6-deoxy-6-fluoro-glucose-1-phosphate (6F-Glc-1P) to cotton ovules growing *in vitro*, demonstrating the metabolic incorporation of 6F-Glc into the fibers with enhanced mechanical properties and moisture-retention capacity while emphasizing the role of molecular hierarchical architecture in defining functional characteristics and mechanical properties. This incorporation strategy bypasses the early steps of conventional metabolic pathways while broadening the range of functionalities that can be employed to customize fiber end properties. Our approach combines materials science, chemistry, and plant sciences to illustrate the innovation required to find alternative solutions for sustainable production of functional cotton fibers with enhanced and emergent properties.

INTRODUCTION

Cellulose is the most abundant biopolymer on Earth, produced by a taxonomically diverse range of organisms, including plants, algae, and bacteria.[1,2] Our understanding of cellulose production across different scales is well established through decades of intense research.[1–10] Cotton stands out as one of the most expressive examples of cellulose production, given its vast economic, industrial, and social impact. However, the current cotton industry faces numerous challenges affecting the sector and the livelihoods of millions of people, prompting the need to explore sustainable medium- to long-term solutions. For example, current methodologies for cellulose modification, especially in cotton, have been largely confined to traditional chemical treatments,[11] which often involve environmentally hazardous processes and limit the potential of cellulose-based materials.[2,12,13]

In response to these challenges, previous knowledge of cotton biosynthetic pathways or enzymatic approaches[14] to cellulose production can be leveraged, presenting promising strategies to create new bio-design landscapes that introduce chemically synthesized building blocks into the end product to tailor and program fiber properties that surpass those of the parent material (e.g., raw cotton fibers).

[1]Department of Plant and Environmental Sciences, Weizmann Institute of Science, Rehovot, Israel

[2]Manchester Institute of Biotechnology and Department of Chemistry, University of Manchester, Manchester, UK

[3]Department of Chemical Research Support, Weizmann Institute of Science, Rehovot, Israel

[4]Ilse Katz Institute for Nanoscale Science & Technology, Ben-Gurion University of the Negev, Beer Sheva, Israel

[5]Institute for Materials Chemistry & Research, Polymer and Composite Engineering Group (PaCE), Universität Wien, Vienna, Austria

[6]SIMS laboratory, Shared Equipment Authority, Rice University, Houston, TX, USA

[7]Department of Food Science, University of Copenhagen, Copenhagen, Denmark

[8]Niels Bohr Institute, University of Copenhagen, Copenhagen, Denmark

[9]Iceni Glycoscience Ltd, Norwich Research Park, UK

[10]These authors contributed equally

[11]Lead contact

*Correspondence: filipe.natalio@weizmann.ac.il

https://doi.org/10.1016/j.xcrp.2024.101963

The cellulose biosynthetic pathway in cotton[6] extensively overlaps with central carbon metabolism, starting with phosphorylation by hexokinase(s) of glucose, actively transported into the intracellular space by glucose transporter(s), followed by transfer of the phosphate group from position C6 to the anomeric carbon (C1). This is finally transformed to the uridine diphosphate form that can be used in general and essential glycosylation reactions or, in the case of cotton fibers, used by a membrane-bound cellulose synthase to polymerize cellulose fibers to the extracellular space. However, the metabolites for each step of this pathway are metabolized, catabolized, and distributed in a complex metabolic network. For example, we recently demonstrated feeding chemo-synthesized 6-deoxy-6-fluoro-glucose (6F-Glc) to the *Gossypium hirsutum in vitro* cotton ovules resulted in the degree of substitution of 0.006, which is 170 times lower than that reported for chemical methods for cellulose modification, highlighting the use of biological systems to introduce low quantities of new functionalities, while maximizing the impact on fiber properties and the role of biological adaptability in "rerouting" of an apparently central carbon-metabolism-incompatible metabolite.[15]

The use of glucose derivatives that bypass some metabolic steps has been explored less, limited by the synthetic methods and the biochemical barriers (e.g., the increase of negative charges by phosphorylation and limited transport). However, it could increase the efficiency of targeted delivery while allowing the introduction of different chemistries.

We recently chemo-synthesize 6-deoxy-6-fluoro-glucose-1-phosphate (6F-Glc-1P) as a donor substrate for the generation of fluorinated cellodextrins (to ~dp 9),[16] resulting in the assembly of narrow fibers of fluorinated cellodextrins with different allomorphs structures to native cellulose.[17–19] We rationalized that combination of 6F-Glc-1P with the fertilized cotton (*G. hirsutum*) ovule *in vitro* culture, could bypass the first step of phosphorylation by hexokinase and facilitate 6F-Glc integration into cotton fibers, opening the doors for expanding the range of functionalities that can be biologically incorporated into cellulose fibers.[20,21] In this manuscript, we present the feeding of 6F-Glc-1P to cotton ovules growing *in vitro*, resulting in incorporation of 6F-Glc into the fiber cellulose network, leading to alterations in the cellulose structure and composition. Such alterations contribute to the production of fibers with enhanced mechanical and moisture-retention properties. This work is expected to advance our understanding of uptake and incorporation mechanisms in the ovules and the future implementation of cotton-fiber modification in the whole cotton plant.

RESULTS

Chemoenzymatic synthesis of 6F-Glc-1P

We reasoned that synthetic 6F-Glc-1P, exogenously fed to fertilized cotton ovules growing *in vitro*, would bypass the need for phosphorylation at position C6 of the glucose moiety by hexokinase and result in incorporation of 6F-Glc into cellulose fibers. The expectation was that this, in turn, would lead to modification of the resulting cellulose fiber properties. To this end, 6F-Glc-1P was synthesized similarly to our previous work.[16] In this current approach (Figure 1A), the first step was performed enzymatically, resulting in a shorter route. Briefly, regioselective deacetylation of the 6-*O*-acetyl group from commercially available α-D-glucose pentaacetate with *Candida rugosa* lipase[22] gave primary alcohol **1** in high yield, thus circumventing extensive use of protecting groups to selectively access the C6 position by chemical means. Conventional direct fluorination of the primary alcohol with diethylaminosulfur trifluoride (DAST) afforded **2** in reasonable yield (unoptimized).[23]

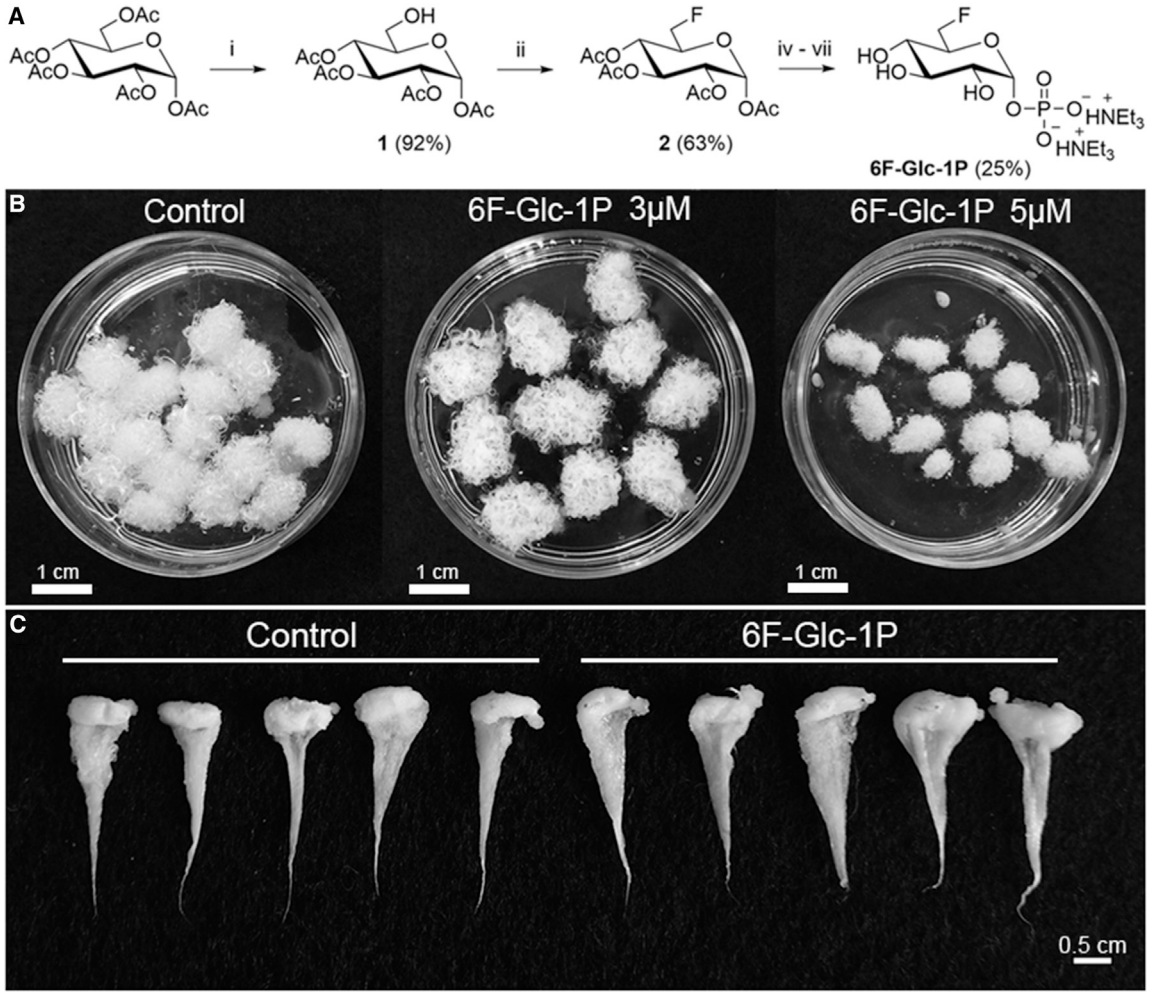

Figure 1. Feeding fertilized cotton ovules *in vitro* with synthetic 6F-Glc-1P

(A) Chemoenzymatic route to the synthesis of 6F-Glc-1P: (i) lipase, phosphate buffer pH 4, dioxane, 24 h at 30°C; (ii) DAST, collidine, DCM; (iii) $AcOH.NH_2NH_2$, DMF; (iv) *n*-BuLi, $(PhO)_2POCl$, THF, −78°C to RT; (v) PtO_2, $H_{2(g)}$, EtOH, 24 h at RT; (vi) Et_3N:H_2O:MeOH (1:3:7, v/v/v), 48 h at room temperature.

(B) Representative photographic image of fertilized *G. hirsutum* ovules *in vitro* cultures, with either no supplement (control, left) or incubated with 6F-Glc-1P at concentrations of 3 μM (middle) and 5 μM (right) after 20 days under standard growth conditions showing altered development of the fibers' total volume and ovules sizes at a concentration of 5 μM. Scale bar, 1 cm.

(C) Representative images of cotton ovules with the combed fibers after standard growth conditions in the absence (left set) or presence of 3 μM 6F-Glc-1P (right set). Scale bar, 0.5 cm. None of the measurements shows a statistically significant difference between control and 6F-Glc-1P ovules and fibers (N = 10, Student's T, $p > 0.05$), while variance was found homogeneous between groups (Brown-Forsythe, $p > 0.05$).

Anomeric deacetylation was carried out with hydrazine acetate ($AcOH.NH_2NH_2$) to give the corresponding hemiacetal, followed by its phosphorylation with diphenyl phosphoryl chloride ($(PhO)_2PO.Cl$). Phenyl deprotection under standard hydrogenation conditions and acetyl cleavage under basic conditions afforded 6F-Glc-1P as triethylammonium salt in 25% yield over the last four steps. It is important to mention that 6F-Glc-1P can also be obtained from α-D-glucose pentaacetate through MacDonald phosphorylation.[24]

Exogenous feeding of 6F-Glc-1P and its impact on fertilized cotton ovules in *in vitro* culture development and growth

We fed two different concentrations of 6F-Glc-1P (3 and 5 μM) to the growth medium of fertilized cotton ovules in *in vitro* cultures. The lower 6F-Glc-1P concentration

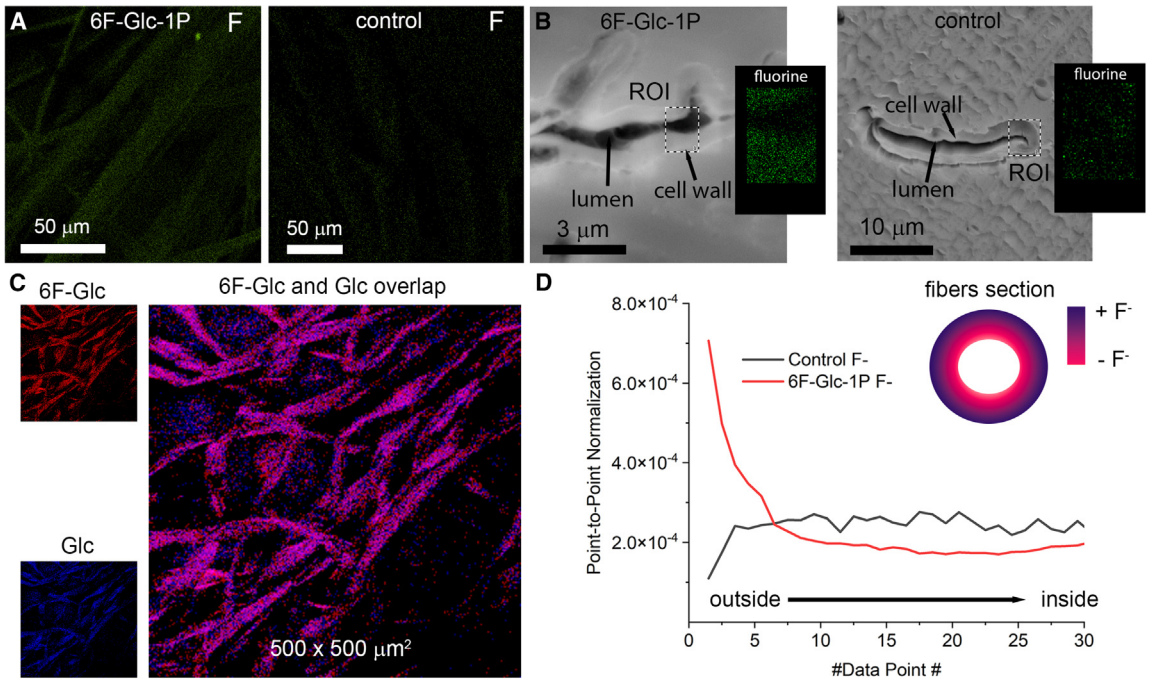

Figure 2. Fluorine content and distribution in modified cotton fibers

(A and B) Elemental analysis fluorine mapping of 6F-Glc-1P fibers (A, left) and control fibers (right) and corresponding cross-sections (B, left for 6F-Glc-1P fibers and right for control fibers). Fluorine was only detected along the fibers and corresponding cross-sections with a homogeneous distribution. Scale bars, 50 μm (A), 3 μm (B, left), and 10 μm (B, right).

(C) ToF-SIMS images of the 6F-Glc-1P fibers using normalized *m/z* 180 and 181 in red and *m/z* 182 and 183 in blue corresponding to 6F-Glc and Glc, respectively (smaller images). Overlay mapping of the 6F-Glc and Glc ions on the same position as described in the smaller images and following the same color code.

(D) Depth profile of the chemical distribution of the F^- ions from the surface inward of the cotton fibers for the control (black line) and the 6F-Glc-1P (red line), respectively. Inset: illustration representing the distribution of fluorine along the fiber cell wall.

leads to a generally lower cotton fiber density but larger total ovule volume than the control (Figure 1B). In contrast, the higher concentration of 6F-Glc-1P (5 μM) causes a decrease in total fiber volume (Figure 1B). We measured and compared ovule size, dry matter content, fiber length, and dry mass between control ovules and those grown in 3 μM 6F-Glc-1P. We found, for all measurements, no statistically significant differences between them (Figure S1) ($N = 10$ per treatment, Student's T, $p > 0.05$), while variance was found to be homogeneous between groups (Brown-Forsythe, $p > 0.05$). Henceforth, the fibers excised from cotton ovules fed with 3 μM 6F-Glc-1P will be referred to as 6F-Glc-1P fibers and those excised from the ovules grown in the absence of any additives as control fibers.

6F-Glc and fluorine are detected inside cotton fibers

Fluorine mapping along the fibers and the corresponding cross-sections shows a relatively homogeneous distribution of fluorine in the 6F-Glc-1P fibers (Figures 2A and 2B, left images). In contrast, no fluorine was found for control fibers and in the cross-sections (Figures 2A and 2B, all right images). We found 0.115 ± 0.02 wt % fluorine content in the 6F-Glc-1P fibers, representing a degree of substitution of 0.01; i.e., for every 100 anhydroglucose units, one hydroxyl group has been substituted. We performed time-of-flight secondary ions mass spectrometry (ToF-SIMS) analysis of the 6F-Glc-1P fibers to putatively identify the chemical nature of the signal. In 6F-Glc-1P fibers, we observed a higher quantitative intensity difference in fiber chemical distribution of 6F-Glc compared to the control fibers (Figure 2C).

We did not find any characteristic ion signal corresponding to 6F-Glc-1P (Figures S2; S3), excluding the possibility of surface contamination. Thus, these results suggest that 6F-Glc-1P has been metabolized and accumulated as 6F-Glc in the fiber.

The depth profile of both control and 6F-Glc-1P fibers for F^- (*m/z* 18.99) showed higher concentration of fluorine at the surface, declining inward in the direction of the lumen (Figure 2D and inset), suggesting a larger 6F-Glc uptake at early stages of fiber development.

6F-Glc-modified cotton fibers reveal an altered morphology and structure

A comparative morphological analysis using scanning electron microscopy (SEM) showed that the 6F-Glc-1P fibers are statistically significantly narrower, about 30%, and less electron transparent than control fibers (Figure S4 and Note S1). To infer whether the presence of 6F-Glc interferes with the H-bonding network of cellulose, we performed a comparative Fourier transform infrared (FTIR) spectroscopy analysis of the 6F-Glc-1P fibers and control fibers. In the spectral region between 3,800 and 3,000 cm^{-1} typically attributed to cellulose intramolecular ((2)H–O(6), O(3)H–O(5)) and intermolecular (O(6)H–O(3)) H-bonds,[25–28] we found that the two intramolecular H-bonds are slightly red shifted in 6F-Glc-1P compared to control fibers. In contrast, the intermolecular H-bond in 6F-Glc-1P fibers is blue shifted (lower wavenumbers) compared to control fibers (Figures 3A and S5). These results indicate a weakening of the interactions within the same cellulose polymer chains and a strengthening of the H-bonds between neighboring cellulose polymer chains,[26] potentially promoted by the presence of additional water molecules and/or by the interaction with the electronegative fluorine atoms from the 6F-Glc moiety. In terms of distance, this likely means that the average distance between atoms within the same polymer chain increases (weakening effect), while the distance between atoms in neighboring chains decreases (strengthening effect), enhancing the material's mechanical properties.

Wide-angle X-ray scattering (WAXS) diffraction patterns of 6F-Glc-1P point to recrystallization with a slight increase of the crystallinity index from 54.4% to 59.3% crystallinity compared to control (Figure S6). This increase in the crystallinity index could be attributed to the formation of additional H-bonds between the fluorine-containing nanofibrils and the OH groups of the neighboring nanofibrils during the extracellular self-assembly, in agreement with the FTIR results and contributing to the enhancement of the material's mechanical properties. The crystallinity index increase found in the 6F-Glc-1P fibers contrasts with previous work where two synthetic glucose derivatives (6-carboxyfluorescein-glucose and dysprosium-1,4,7,10-tetraazacyclododecane-1,4,7,10-tetraacetic acid-glucose) were incorporated into cellulose fiber in *in vitro* cotton ovule culture models, resulting in cellulose amorphization and decreased crystallinity, due to the size and/or chemistry of the functionalities that interferes negatively with the process extracellular self-assembly of the nanofibrils, leading also to reduced mechanical (tensile) properties.[21] Figure 3B shows that the WAXS diffraction pattern of the 6F-Glc-1P fibers fits deceptively well to a cellulose $I_{III\ I}$ allomorph,[29] with the main peak corresponding to the $1\bar{1}0$ reflection, perhaps with some remnants of the cellulose I_α and I_β allomorphs still present, indicated by the broad shoulder around $q \sim 1.2$ $Å^{-1}$. However, the low degree of substitution does not immediately suggest the presence of the cellulose $I_{III\ I}$ allomorph, which typically forms through the diffusion of water after ammonia infiltration, leading ultimately to fiber swelling.[30] Thus, based on the current data, we cannot unambiguously assign this modification to the allomorph cellulose $I_{III\ I}$ at this time.

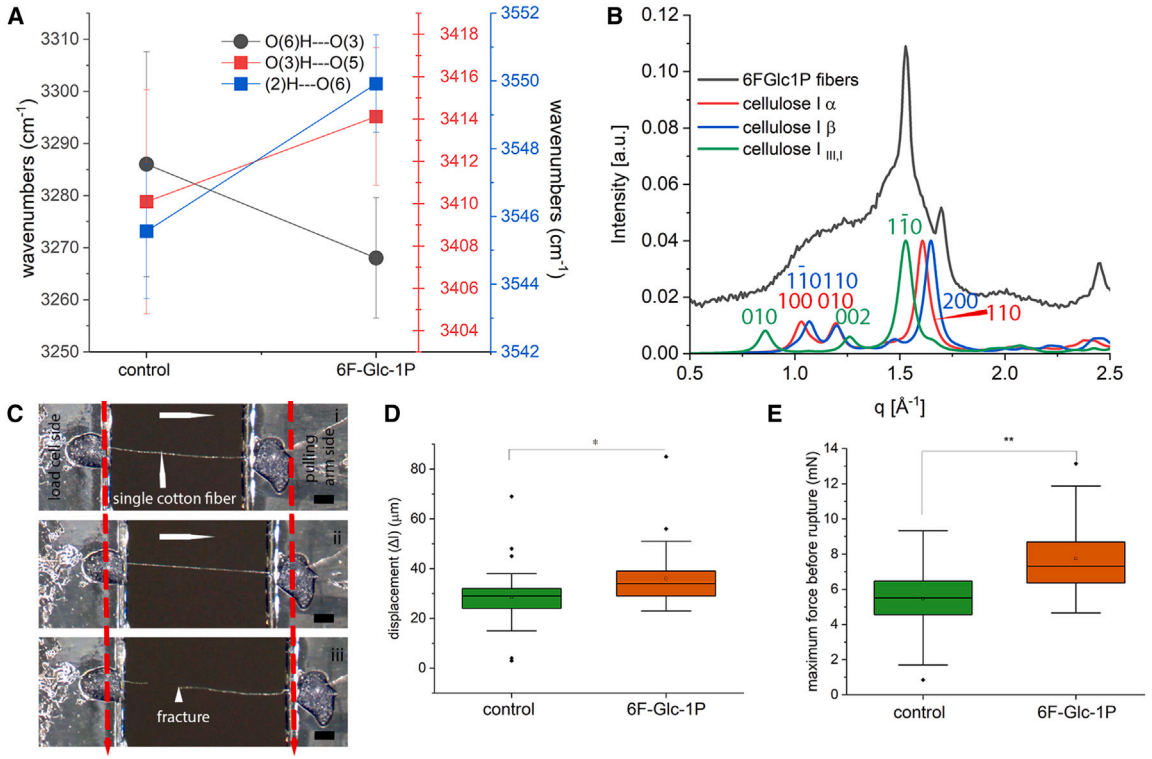

Figure 3. Structural and mechanical characterization of the modified cotton fibers

(A) Maximum peaks variation of two intramolecular ((2)H–O(6) [blue squares], O(3)H–O(5) [red squares]) and one intermolecular (O(6)H–O(3), gray circles) hydrogen bonds in 6F-Glc-1P fibers compared to control fibers, indicating a reorganized H-bond network with stronger intermolecular and weaker intramolecular bonds.

(B) WAXS diffraction data from 6F-Glc-1P showing it is composed mainly of cellulose $I_{III\ I}$-like allomorph with cellulose I_α/I_β allomorphs. Simulated diffraction curves based on crystallographic data for cellulose allomorphs are shown under the experimental WAXS diffraction curves. Color code and three lowest crystal plane families for each are as follows: blue line, cellulose I_α [100], [010], [110]; green line, cellulose I_β [1–10], [110], [200]; and purple line, cellulose $I_{III\ I}$ [010], [002], [1$\bar{1}$0].

(C) Light microscopy sequence of a single 6F-Glc-1P fiber during tensile testing: (i) initial stretch, (ii) pre-fracture maximum force/displacement, and (iii) post-fracture (white arrow). The horizontal white arrow shows the direction of the end being pulled. Scale bar, 200 μm.

(D) Box-plot of displacement calculated for control and 6F-Glc-1P fibers. The 6F-Glc-1P fibers show a statistically significantly larger displacement (ANOVA, $N = 40$ for each treatment, $p < 0.05$) than control fibers, with values of 36 ± 10.81 μm and 28.53 ± 10.86 μm for 6F-Glc-1P and control fibers, respectively.

(E) Box-plot of the maximum forces required for fracturing single control and 6F-Glc-1P fibers. The mean maximum force for disrupting single cotton 6F-Glc-1P fibers was statistically significantly higher than control fibers (ANOVA, $N = 40$ for each treatment, $p < 0.05$), exhibiting a 1.42-fold increase.

6F-Glc-modified cotton fibers exhibit enhanced mechanical properties

To assess the mechanical properties of cotton fibers, we performed single-fiber tensile testing (Figure 3C i–iii for 6F-Glc-1P; Figure S7 for control fibers, and corresponding videos can be found in supplemental information as Video S1 for control and Video S2 for 6F-Glc-1P). We determined the displacement prior to fracture of the 6F-Glc-1P fibers to be statistically significantly larger than control fibers (ANOVA, $N = 40$ for each treatment, $p < 0.05$). Specifically, 6F-Glc-1P and control fibers show a mean displacement of 36 ± 10.81 μm and 28.53 ± 10.86 μm, respectively (Figure 3D). In both cases, we find a large dispersion attributed to the natural variability of the tensile properties of the single fibers overshadowed by the classical bulk-fiber tensile analyses. The mean maximum forces required for single-cotton-fiber fracture are statistically significantly higher by 1.42-fold between 6F-Glc-1P and control fibers (ANOVA, $N = 40$ for each treatment, $p < 0.05$). Specifically, we calculated a mean maximum force before fiber rupture of 5.46 ± 1.8 mN and 7.74 ± 2.1 mN for control and 6F-Glc-1P fibers, respectively (Figure 3E). This observed

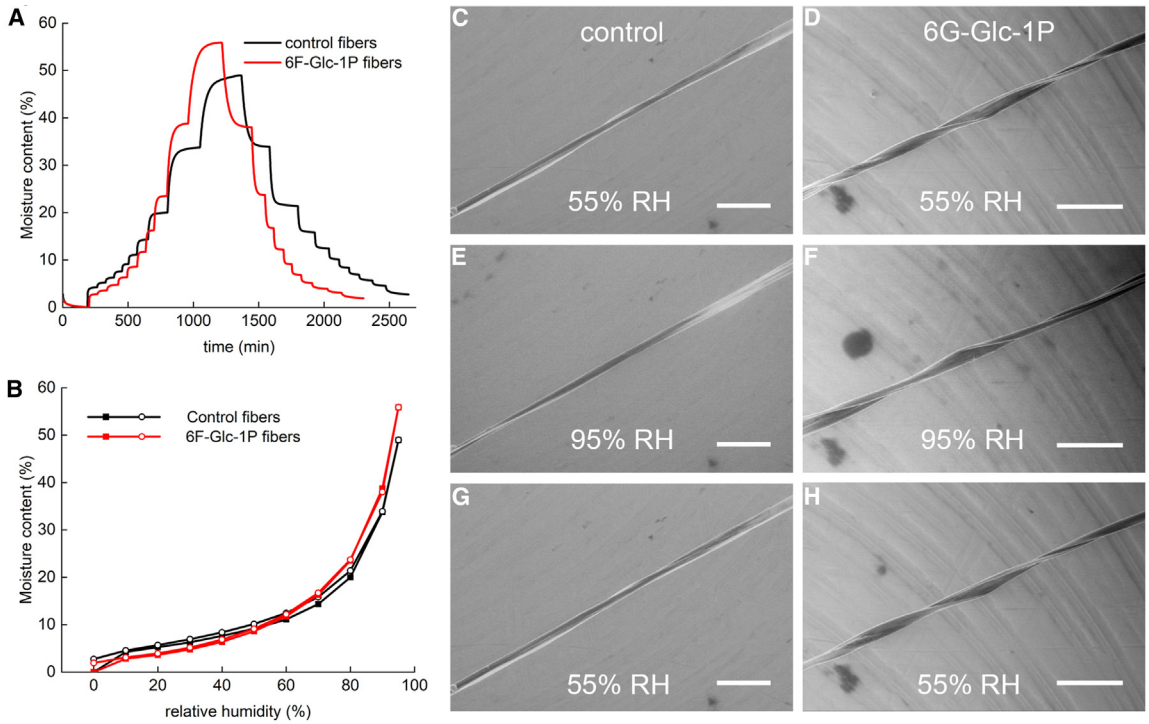

Figure 4. DVS and moisture retention in cotton fibers

(A) Water vapor sorption kinetics of control and 6F-Glc-1P fibers plotted as the moisture content (weight) vs. function of relative humidity, cycling from 0% to 95% RH, then back to 0% RH. Control (black line) and 6F-Glc-1P fibers (red line) exhibit maximum moisture-retaining capacity of 48.96% and 55.88% at 95% RH, respectively.

(B) Sorption isotherm curves obtained from plotting the moisture content at the equilibrium moisture content (EMC) vs. relative humidity for the control (black line) and 6F-Glc-1P fibers (red line), cycling from 0% to 95% RH, then back to 0%. Lines with solid squares correspond to adsorption curves, while lines with hollow circles correspond to desorption curves. Both control (black line) and 6F-Glc-1P fibers show a type II isotherm sorption profile with more pronounced differences at higher humidity regimes.

(C–H) Morphological assessment of single control and 6F-Glc-1P fibers at different relative humidities (C and D, 55% RH; E and F, 95% RH; and G and H, 55% RH) analyzed by ESEM. As the RH increases, all fibers start to swell and untwist/deconvolute. No water droplets are formed on the fiber's surface. In contrast to the control fibers, which are fully swollen at 95% RH, the 6F-Glc-1P fibers partially retain their initial morphology (E and F). Only control fibers reverted to the initial morphology when RH was decreased to 55% RH (G and H). Scale bar (C–H), 50 μm.

increase in the mean maximum force before fiber rupture for the 6F-Glc-1P fibers is attributed to an increase in the compactness and stability of the overall cellulose network between adjacent cellulose chains, due to the fluorine-altered H-bond network, as indicated by the FTIR and WAXS data, preventing nanofibrils from shearing under tension.

Single and bulk 6F-Glc-modified cotton fibers exhibit enhanced moisture-retaining properties

To assess the effect of the presence of 6F-Glc in the fibers on the moisture-retaining capacity, we performed dynamic vapor sorption (DVS) measurements with a variation of relative humidity from 0% to 95% and then back to 0% on a bundle of control and 6F-Glc-1P fibers. From the kinetic profile, we found that, at 95% relative humidity (RH), 6F-Glc-1P fibers exhibit a 7% increase in their capacity to retain more moisture (Figure 4A, red line) than control fibers (Figure 4A black line). In both cases, the sorption isotherms have a hysteresis shape, typically attributed to a type II isotherm (Figure 4B), with 6F-Glc-1P fibers displaying higher equilibrium moisture content (EMC) at higher humidity levels than control fibers (Note S2).

In a further step, we investigated the morphological changes the fibers undergo under different RH conditions using *in situ* swelling experiments in an environmental scanning electron microscope (ESEM). The increase of RH from 55% RH to 95% resulted in swelling and untwisting/deconvoluting of the fibers (Figures 4C–4H), and their surface became smoother. In both cases, this process did not result in water condensation on the fiber's surface. At 95% RH, the 6F-Glc-1P fibers are swollen but still preserve their deconvolutions (Figure 4E), in contrast to fully swollen control fibers (Figure 4F). We found that 6F-Glc-1P fibers only revert to their initial morphology when RH is further reduced to 45% RH, whereas the control fibers fully recover their morphology at 55% RH (Figure S8).

Incorporation of 6F-Glc into the cellulose structure leads to a reorganization of H-bonds that reduce the distance between cellulose nanofibrils, increasing the crystallinity and making the network denser and more compact. However, this modified cellulose structure has limited space available for water molecules to penetrate or be accommodated within the cellulose structure, in contrast with our data. While this could be attributed to the presence of cellulose $I_{III\ I}$-like allomorph characterized by a larger unit cell volume than native cellulose I α or β[29], our data emphasize the role of molecular hierarchical architecture of cellulose fibers over solely altering the crystalline and amorphous regions and/or H-bond network modification in defining fiber properties.

DISCUSSION

Leveraging biological systems to explore biological materials design landscapes, offering novel and tailored properties with industrial, economic, and environmental benefits, has become increasingly prominent. This trend is driven by significant advances in synthetic biology, particularly in prokaryotes and, more recently, eukaryotes. In this study, we capitalized on the natural biosynthetic machinery of cotton and steered it to introduce new functionalities into cotton cellulose fibers. One key aspect of our research is the deployment of synthetic 6F-Glc-1P to bypass early steps of the cellulose biosynthetic pathway using a multicellular organism (cotton) *in vitro*. This endows cotton fibers with emergent properties while broadening the spectrum of functionalities that can be introduced into such fibers and reducing potential catabolic processes and inhibitory effects on the enzymes involved.[31] Improvement in the mechanical and moisture-retaining properties of the fibers formed in this way surpassed those available in raw cotton fibers, advocating a role for the molecular hierarchical architecture in cellulose fibers beyond mere adjustments to the crystalline and amorphous regions, or modifications in the H-bonding network, in defining their functional characteristics and mechanical properties.

As yet, these *in vitro* experiments are limited with respect to real-life application potential. However, the physiological and biochemical uniqueness and the complexity of the ovule are the core of fiber growth and development of cotton plants (Figure 5). Thus, our experiments provide an insightful new contribution to our understanding of regulatory and transport mechanisms at the ovule level, unraveling potential new approaches to modify the fibers in the whole cotton plant, by employing glucose derivatives as substrates. These approaches include, for example, the upscale of chemoenzymatic synthesis of 6F-Glc-1P, feeding it to the roots of hydroponically grown cotton, and exploring the level of incorporation in the cotton fibers (Figure 5). This approach could represent a breakthrough in biologically designed, sustainable, multifunctional, and enhanced cotton cellulose fibers for real-life applications

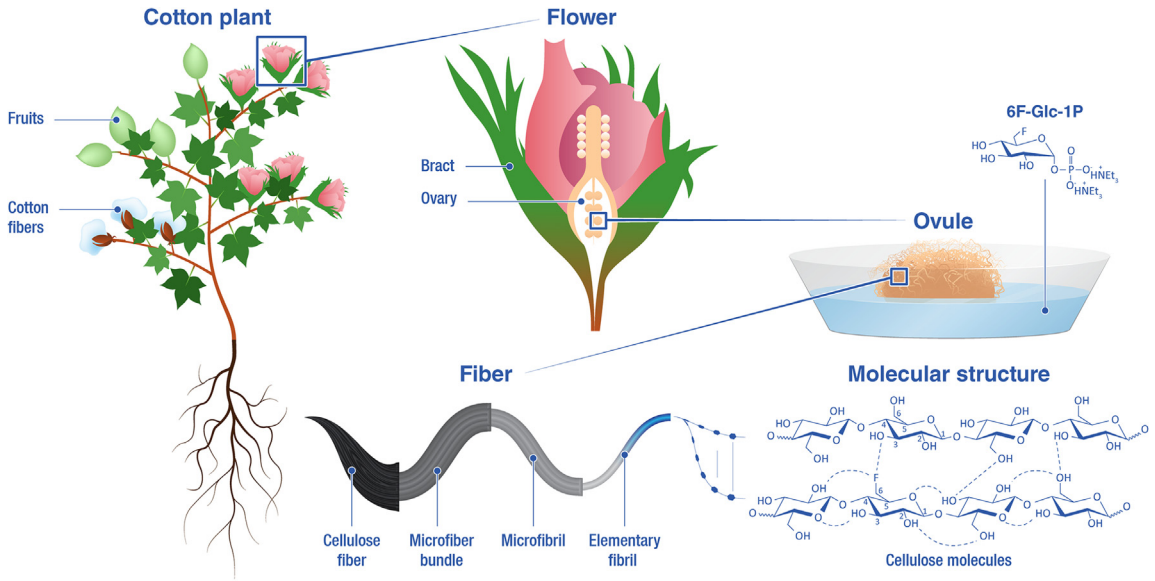

Figure 5. Deconvoluting hierarchical complexity material farming: From ovules to the whole cotton plant

Schematic representation of the conceptual translational roadmap from the molecular structure of cellulose to the whole plant toward the implementation of the concept of material farming and to biologically design cotton fibers with tailored properties. This report, while showing the presence of chemically synthesized 6F-Glc-1P and its incorporation into cotton fibers using the cotton ovule *in vitro* culture, represents a step forward in increasing our understanding of this process and moves one step closer to the translation of the material farming framework into real-life contexts to serve as a sustainable alternative to current textile-dyeing practices.

toward the implementation of the concept of material farming in alignment with the principles of green chemistry.[32]

EXPERIMENTAL PROCEDURES

Resource availability

Lead contact

Further information and requests for resources should be directed to and will be fulfilled by the lead contact, Filipe Natalio (filipe.natalio@weizmann.ac.il).

Materials availability

This study did not generate new unique reagents.

Data and code availability

The data used to support the findings of this study are publicly available at: https://github.com/fnatalio/Bypassing6F or https://doi.org/10.5281/zenodo.10932851

Chemoenzymatic synthesis of 6F-Glc-1P derivative

C. rugosa lipase (2.5 g) (type VII, >700 unit/mg solid, L1754, Sigma-Adrich, United Kingdom) was added to a suspension of α-D-glucose pentaacetate (5.0 g, 12.82 mmol) in a mixture of 1,4-dioxane (100 mL) and phosphate buffer pH 4 (500 mL at 30 mM), and the reaction was kept under shaking (250 rpm) at 30°C for 24 h. The suspension was centrifuged, and the supernatant was extracted with EtOAc (3 × 100 mL), dried over $MgSO_4$, filtered, concentrated under reduced pressure, and purified by column chromatography (hexane/EtOAc 4:6) to give compound **1** (4.1 g; 11.80 mmol; 92%).[22] The following steps were performed as described in our previous work.[16] Briefly, compound **1** (4.1 g; 11.80 mmol) was dissolved in anhydrous DCM (100 mL) under N_2, and collidine (3.15 mL; 23.60 mmol) was added. The mixture was cooled to −20°C, DAST (3.15 mL; 23.60 mmol) was

added dropwise over 15 min, and the reaction was stirred at RT for 24 h. The reaction was quenched with MeOH (20 mL), concentrated under vacuum, and purified by column chromatography (DCM/EtOAc 9.5:0.5) to give compound **2** (2.60 g; 7.43 mmol; 63%).[23] Hydrazine acetate (420 mg; 4.57 mmol) was added to a solution of compound **2** (1.6 g; 4.57 mmol) in anhydrous DMF (10 mL) under N_2 and stirred at RT overnight. The hemiacetal intermediate was obtained (850 mg; 2.76 mmol; 60%) after workup and purification. To a solution of the hemiacetal (822 mg; 2.67 mmol) in anhydrous THF (40 mL) at −78°C under N_2, *n*-BuLi (2 mL in hexane; 3.20 mmol) was added dropwise followed by dropwise addition of diphenyl phosphoryl chloride (664 μL; 3.20 mmol). After 16 h at RT, the reaction was quenched with NH_4Cl solution, partitioned with EtOAc, and purified by flash chromatography to give the diphenylphosphate intermediate (690 mg; 1.28 mmol; 48%). The phenyl cleavage of this intermediate (600 mg; 1.11 mmol) was carried out with PtO_2 (50 mg; 0.22 mmol) in absolute ethanol (25 mL) at RT under an H_2 atmosphere for 48 h. The acetyl cleavage of the crude phosphate was performed in Et_3N:H_2O:MeOH (1:3:7, v/v/v) (45 mL) under stirring for 48 h at RT. After the solvents' removal under vacuum, the residue was dissolved in water and freeze-dried to afford 6F-Glc-1P as triethylammonium salt (457 mg; 0.98 mmol; 88%).

Cotton growth conditions and fertilized *in vitro* ovule cultures

Cotton (*G. hirsutum*) was grown in soil in a greenhouse between November 2021 and February 2022 at the Weizmann Institute of Science greenhouse facilities. Flowers were harvested 2 days post anthesis (2 dpa), and the ovary was sterilized in a solution of NaOCl (6%) for 2 min at room temperature. The fertilized ovules were aseptically removed and placed floating onto sterile Beasley and Ting (BT) medium (15 mL) supplemented with gibberellic acid (GA, 5 μM, Sigma, Germany), indoleacetic acid (IAA, 0.5 μM, Germany), and additives (see section "ovule feeding experiments"). The cultures were kept in the dark at 30°C and 5% CO_2 for 20 days (standard conditions).[33,34]

Ovule feeding experiments

Chemo-synthesized 6F-Glc-1P (3 and 5 μM) were mixed with sterile BT medium supplemented with phytohormones (5 μM of GA and 0.5 μM IAA) and fed to *G. hirsutum* ovules collected at 2 dpa. The ovules were kept under standard conditions (dark at 30°C and 5% CO_2 for 20 days). Afterward, the cotton ovules were harvested. The fibers were carefully removed with the help of a sterile scalpel, washed five times with double-distilled water, and placed at −80°C until further characterization.

Measurements of ovule length and weight and fiber length

Following the 20-day growth period under standard conditions, ovules of control and 6F-Glc-1P were washed extensively in double-distilled water to remove any excess medium and were allowed to air-dry in a biological flow chamber. Measurements of ovule length and weight, and fiber length were carried out as described elsewhere.[35] Once dry, ovules were weighed and placed in boiling distilled water for 2 min to relax the fibers. Next, each ovule was held under a running tap to straighten the fibers and dragged on filter paper to dry and align all fibers in the same direction. Aligned fibers were imaged using a Canon EOS M5 camera, and ovule and fiber length were measured using ImageJ software. Once imaged, ovules were placed in an oven at 50°C overnight to desiccate and weighed again the following day for dry-matter content calculations. Next, the fiber bundle was carefully separated using a stainless steel scalpel and weighed separately. All statistical analysis was performed and plots were created using JASP software (v 0.16.4) from independent measurements.[36]

ToF-SIMS

ToF-SIMS measurements were performed using a TOF-SIMS NCS instrument, which combines a TOF.SIMS5 instrument (ION-TOF, Münster, Germany) and an *in situ* Scanning Probe Microscope (NanoScan, Switzerland) at Shared Equipment Authority from Rice University.

Surface spectrometry

A bunched 30 keV Bi_3^+ ion (with a measured current of 0.15 pA) was used as the primary probe for analysis (scanned area 500 × 500 μm^2) with a raster of 128 × 128 pixels. A charge compensation with an electron flood gun was applied during the analysis. The charge effects have been adjusted using appropriate surface potential and adapted extraction bias depending on the analysis area and the polarity. The cycle time was fixed to 100 μs (corresponding to m/z = 0–911 a.m.u. mass range). The primary ion dose density was limited to 1.10^{12} ions/cm^2 to preserve the analyzed surface.

Two-dimensional imaging

A bunched 60 keV Bi_3^+ ions (with a measured current of 0.05 pA) was used as the primary probe for imaging a field of view of 500 × 500 μm^2, with a raster of 2048 by 2048 pixels, and then the image raster was binned by a factor 64 to enhance the signal-to-noise ratio. A charge compensation with an electron flood gun was applied during the analysis. An adjustment of the charge effects has been operated using a surface potential. The cycle time was fixed to 70 μs (corresponding to m/z = 0–446 a.m.u. mass range).

Depth profiling

A bunched 30 keV Bi_3^+ ions (with a measured current of 0.15 pA) was used as the primary probe for depth profiling a field of view of 150 × 150 μm^2, with a raster of 64 by 64 pixels, and then the sputtering was performed using Ar_{1500}^+ ions at 10 keV with a typical current around 2.5 nA, rastered area of 500 × 500 μm^2. The beams were operated in non-interlaced mode, alternating one analysis cycle and one sputtering cycle (corresponding to 3.28 s) followed by a pause of 5 s for the charge compensation with an electron flood gun. Again, the charge effects were adjusted using a surface potential. During the depth profiling, the cycle time was fixed to 200 μs (corresponding to m/z = 0–3645 a.m.u. mass range).

Data treatment

All of the data have been treated and extracted using SurfaceLab 7.3. Ion signals from spectra and from ion mappings have been normalized using the total ion signal to standardize the values and to help compare the different samples or the area. A logarithmic color scale was used when the ion signal was too low to identify the local variations.

Cross-sections preparation

The 6F-Glc-1P and control fibers were aligned and embedded in epon EMbed 812 (EMS #14120) and polymerized in a mold for 24 h at 60°C. Thin sections were prepared with an ultra-microtome (Leica UCT, Germany), collected onto a carbon stub, and further analyzed as described below.

Elemental analysis and degree of substitution

Washed fibers excised from ovules fed with 6F-Glc-1P (3 μM) and control were air-dried. Fibers and respective cross-sections were glued onto a carbon stub. For elemental analysis, the elemental analysis dispersive X-ray (EDS) analysis built in

from the Phenom XL was used with an acceleration voltage of 15 kV and vacuum 1 Pa and point as spot size. The data were collected in points on different 6F-Glc-1P or control fibers (N = 10) or two-dimensional (2D) maps. The degree of substitution (DS) was calculated using the formula (Equation 1)[37,38] adapted to fluorine:

$$DS = \frac{MGlc.wt\%\ F}{100Mn - Mmat.wt\%F} \quad \text{(Equation 1)}$$

where MGlc is the molar mass of the anhydroglucose unit (162 g/mol), Mn is the molar mass of the fluorine atom, Mmat is the molar mass of the fluorine introduced into the cellulose,[37,38] and wt%F is the fluorine content determined by elemental EDS analysis.

FTIR spectroscopy

The samples were analyzed by FTIR spectroscopy. The samples were powdered and mixed with 5 mg of KBr. The mixture was pressed into a 7-mm die using a Pike hand press and analyzed with a Thermo Nicolet iS5 FTIR spectrometer. FTIR spectra were collected by performing 32 scans with a resolution of 4 cm^{-1} wavenumbers. The FTIR spectra were collected using Omnic software. Measurements were performed at room temperature and in triplicates. The data were replotted and peak fitted using OriginLab Pro 2018 (b9.5.0193) using Gauss as peak function.

WAXS

WAXS measurements were performed using a Nano-inXider instrument from Xenocs SAS (Grenoble, France) (6F-Glc-1P fibers). The instrument was equipped with a Rigaku (Rigaku-Denki, Tokyo, Japan) 40-W micro-focused Cu source producing X-rays. A wavelength of λ = 1.54 Å was in both cases detected by a Pilatus detector from Dectris (Baden, Switzerland). The 2D scattering data were radially and azimuthally averaged using standard reduction software (XSACT, Grenoble, France). The scattering patterns for the radially averaged intensity were recorded as a function of the scattering vector (Equation 2)

$$q = 4\pi * \sin\theta/\lambda \quad \text{(Equation 2)}$$

where 2θ is the scattering angle. q was recorded in the range of 0.55–2.45 $Å^{-1}$ in the WAXS configuration. Samples were mounted wet and gently aligned to form a fiber bundle and measured *in vacuo*. Measuring times were 900 s for WAXS. Cellulose WAXS patterns were calculated using the crystallographic data from French[39] using the Mercury package powder pattern calculator with full width at half maximum (FWHM) set to 1°.[40] Crystallinity was estimated using the empirical method of Segal[41] using the ratio of the sharpest reflection intensity to an amorphous region. We used intensities from the following two theta values: control, 23° vs. 19°; 6F-Glc-1P, 21.6° vs. 16.8°.

Single-fiber tensile properties

The mechanical (tensile) tests of single cotton fibers were performed on our home-made push-to-pull tensile tester (Figure S9). The tester setup integrates a nano-manipulator (Kleindiek Nanotechnik, NanoControl NC-2-3), a load cell (Kleindiek Nanotechnik, STFMA SpringTable with the spring constant 106 N/m), and an arm that reverses the pushing force from the nano-manipulator to a pulling force that stretches the sample and deflects the load cell. Individual cotton fibers were carefully separated from a bundle with the help of an optical stereo microscope. The single fiber was then transferred onto a laser-cut polyester sample holder with a 1-mm-diameter window, and both ends of the fiber were then fixed on the edge of the notch (Figure S10) with epoxy glue and allowed to dry for 2 days at room

temperature. The tests were monitored and recorded using a Carl Zeiss SteREO Discovery.V12 stereomicroscope at 26°C and 36% RH. Videos were collected using an AMScope camera and respective acquisition software. It was made sure that both ends of the fiber were visible in the field of view throughout the test. The videos were split into single images. The displacement (Δl) was calculated by subtracting load cell deflection (Δx) from the deflection of the actuator (pulling arm) (a) using the formula (Equation 3)

$$\Delta l = a - \Delta x \quad \text{(Equation 3)}$$

where Δl is the displacement, Δx is the load cell deflection, and (a) is the deflection of the actuator (pulling arm). The values for Δx and a were determined directly from the overlapping images immediately before stretching and immediately before failure using Fiji/ImageJ.[42]

The forces were calculated from the deflection of the load cell (Δx) directly from the overlapping images immediately before stretching and immediately before failure using Fiji/ImageJ.[42] As for the force, we used Hooke's law (Equation 4):

$$F = k * \Delta x \quad \text{(Equation 4)}$$

where k and Δx are the spring constant (106 N/m) and the deflection of the load cell, respectively, assuming the stiffness of the setup is much higher than that of the cotton fiber, and we follow the movement of the fiber end close to the load cell and use it as the deflection of the load cell. For each type of fiber, we measured 40 specimens for statistical reasons. All statistical analyses (descriptive and ANOVA) were performed using JASP software from independent measurements (v 0.16.4).[36]

DVS

Water vapor sorption of the fibers was measured using DVS (DVS Intrinsic, Surface Measurement System, UK). About 5 mg of fibers were placed in a chamber. The temperature in the chamber was controlled to be 25°C. The RH in the chamber was changed stepwise from 0% to 95% and then back to 0% RH with an interval of 10% RH (with the exception of the region ranging from 90% to 95% to 90% RH, which was a 5% RH interval). The mass change of the specimen was recorded as a function of time; when the mass change reached an equilibrium, i.e., <0.002% change and stable for 10 min, the RH changed to the next step. The mass change was plotted as a function of time; the mass change at equilibrium was plotted as a function of RH. The data were replotted using OriginLab Pro 2018 (b9.5.0193).

In situ swelling test under an ESEM

The *in situ* swelling tests on the control and treated cotton fibers were performed under an ESEM (QuattroS, Thermo Fisher Scientific). Individual fibers were separated from the bundle, and both ends of the fiber were carefully fixed on a metal washer by carbon tape. The experiments were performed in the water vapor environment, and samples mounted on a washer were sitting on a Peltier cooling stage set at +4°C for the whole process. Images were acquired at 10 kV, spot size was 3.5 or 4, with a working distance of 10–11 mm, using the secondary electrons (SEs) mode of the gaseous secondary electron detector (GSED) mounted on the pole piece. To perform an *in situ* swelling test, the humidity was controlled by changing the pressure in the chamber. The advantage of using water vapor in these *in situ* swelling experiments is 2-fold. First, it provides a controllable wet environment necessary for testing the swelling properties of biological samples. Second, the water vapor pumped into the chamber is ionized by the electron beam, which can neutralize the charged surface of a non-conductive sample caused by the electron

beam. Therefore, no coating is required before the experiment.[43,44] The imaging conditions were initially optimized to avoid beam damage to the single cotton fibers during the measurements. Under these optimized imaging conditions, we did not observe beam damage on any of the different RH conditions used. The samples were inserted in the chamber at 55% humidity, and then the swelling test was done in a dry-wet-dry cycle, meaning the chamber humidity was set to 55%-95%-55% with 5% intervals. To minimize the beam damage, instead of recording a continuously monitored video, the electron beam was blocked between the humidity points, and images were only taken after the humidity stabilized at each point. The images were then combined and formed a video by the software Fiji/ImageJ.[42]

SUPPLEMENTAL INFORMATION

Supplemental information can be found online at https://doi.org/10.1016/j.xcrp.2024.101963.

ACKNOWLEDGMENTS

We want to thank Dr. Samuel Bodé and Dr. Katja Van Nieuland (Isotope Bioscience Laboratory (ISOFYS), Faculty of Bioscience Engineering, Belgium) for their help with EA-IRMS measurements. We want to thank Luis Favas for the illustrations. This work was funded by the European Union, ERC Consolidator project BIOMATFAB (project #101045466); a GIF German-Israeli Foundation for Scientific Research and Development research grant #I-1509-302.5/2019; the MINERVA Stiftung (project # 136809), with the funds from the BMBF of the Federal Republic of Germany, Benoziyo Endowment Fund for the Advancement of Science; a research grant from the Yotam project, the Weizmann Institute Sustainability and Energy Research Initiative (SAERI); the Moskowitz Center at the Weizmann Institute of Science for Nano and Bio-Imaging funding; and the University of Manchester. Views and opinions expressed are, however, those of the author(s) only and do not necessarily reflect those of the European Union or the European Research Council. Neither the European Union nor the granting authority can be held responsible for them. ToF-SIMS analysis was carried out with support provided by the National Science Foundation CBET-1626418. This work was conducted in part using resources of the Shared Equipment Authority at Rice University (USA). Data were generated in part by accessing research infrastructure at University of Copenhagen, including FOODHAY (Food and Health Open Innovation Laboratory, Danish Roadmap for Research Infrastructure).

AUTHOR CONTRIBUTIONS

O.A.K. performed growth cotton ovules *in vitro* experiments, performed single-fiber mechanical testing, and wrote and revised the manuscript. P.A. performed the chemosynthesis of 6F-Glc-1P and wrote and revised the manuscript. X.S. performed the wettability experiments, analyzed and interpreted the data, and wrote and revised the manuscript. R.M. performed the cross-sections and the elemental analysis of the fibers' cross-sections, analyzed and interpreted the data, and wrote and revised the manuscript. I.K.-A. performed the wettability experiments, analyzed and interpreted the data, and wrote and revised the manuscript. Q.J. performed the water sorption dynamics measurements, analyzed and interpreted the data, and wrote and revised the manuscript. T.T. performed the ToF-SIMS analysis of the 6F-Glc-1P and control fibers, analyzed and interpreted the data, and wrote and revised the manuscript. J.J.K.K. performed WAXS analysis 6F-Glc-1P and control fibers, analyzed and interpreted the data, and wrote and revised the manuscript. R.F. performed conceptualization, supervision, management, and funding acquisition and wrote and revised the manuscript. F.N. performed conceptualization,

supervision, management, and funding acquisition and wrote and revised the manuscript.

DECLARATION OF INTERESTS

The authors declare no competing interests.

Received: November 29, 2023
Revised: March 15, 2024
Accepted: April 15, 2024
Published: May 7, 2024

REFERENCES

1. Klemm, D., Heublein, B., Fink, H.-P., and Bohn, A. (2005). Cellulose: Fascinating Biopolymer and Sustainable Raw Material. Angew. Chem., Int. Ed. Engl. *44*, 3358–3393. https://doi.org/10.1002/anie.200460587.

2. Heinze, T. (2015). Cellulose: structure and properties. Cellulose chemistry and properties: fibers, nanocelluloses and advanced materials, 1–52. https://doi.org/10.1007/12_2015_319.

3. Carpita, N.C., and Delmer, D.P. (1981). Concentration and metabolic turnover of UDP-glucose in developing cotton fibers. J. Biol. Chem. *256*, 308–315. https://doi.org/10.1016/s0021-9258(19)70136-7.

4. Delmer, D.P., and Amor, Y. (1995). Cellulose biosynthesis. Plant Cell *7*, 987–1000.

5. Larsen, G.L., and Brummond, D.O. (1974). β-(1→4)-d-glucan synthesis from UDOP-[14C]-d- glucose by a solubilized enzyme from Lupinus albus. Phytochemistry *13*, 361–365. https://doi.org/10.1016/S0031-9422(00)91218-4.

6. Babb, V.M., and Haigler, C.H. (2001). Sucrose phosphate synthase activity rises in correlation with high-rate cellulose synthesis in three heterotrophic systems. Plant Physiol. *127*, 1234–1242. https://doi.org/10.1104/pp.010424.

7. Pérez, S., and Samain, D. (2010). Structure and engineering of celluloses. Adv. Carbohydr. Chem. Biochem. *64*, 25–116. https://doi.org/10.1016/S0065-2318(10)64003-6.

8. Pérez, S., and Mazeau, K. (2005). Conformations, structures, and morphologies of celluloses. Polysaccharides: Structural diversity and functional versatility *2*. https://doi.org/10.1201/9781420030822.

9. Fratzl, P. (2003). Cellulose and collagen: from fibres to tissues. Curr. Opin. Colloid Interface Sci. *8*, 32–39. https://doi.org/10.1016/S1359-0294(03)00011-6.

10. Burgert, I., and Fratzl, P. (2009). Plants control the properties and actuation of their organs through the orientation of cellulose fibrils in their cell walls. Integr. Comp. Biol. *49*, 69–79. https://doi.org/10.1093/icb/icp026.

11. Kant, R. (2012). Textile dyeing industry an environmental hazard. Nat. Sci. *04*, 22–26. https://doi.org/10.4236/ns.2012.41004.

12. Trivedi, P., and Fardim, P. (2019). Recent advances in cellulose chemistry and potential applications. Production of Materials from Sustainable Biomass Resources, pp. 99–115. https://doi.org/10.1007/978-981-13-3768-0_4.

13. Heinze, T., Schwikal, K., and Barthel, S. (2005). Ionic Liquids as Reaction Medium in Cellulose Functionalization. Macromol. Biosci. *5*, 520–525. https://doi.org/10.1002/mabi.200500039.

14. Bulmer, G.S., de Andrade, P., Field, R.A., and van Munster, J.M. (2021). Recent advances in enzymatic synthesis of β-glucan and cellulose. Carbohydr. Res. *508*, 108411. https://doi.org/10.1016/j.carres.2021.108411.

15. Kuperman, O.A., de Andrade, P., Terlier, T., Kirkensgaard, J.J.K., Field, R.A., and Natalio, F. (2023). The Effect of a Low Degree of Fluorine Substitution on Cotton Fiber Properties. Macromolecular Materials and Engineering *n/a*. Macromol. Mater. Eng. *309*, 2300337. https://doi.org/10.1002/mame.202300337.

16. de Andrade, P., Muñoz-García, J.C., Pergolizzi, G., Gabrielli, V., Nepogodiev, S.A., Iuga, D., Fábián, L., Nigmatullin, R., Johns, M.A., Harniman, R., et al. (2021). Chemoenzymatic Synthesis of Fluorinated Cellodextrins Identifies a New Allomorph for Cellulose-Like Materials. Chem. Eur J. *27*, 1374–1382. https://doi.org/10.1002/chem.202003604.

17. Nigmatullin, R., de Andrade, P., Harniman, R., Field, R.A., and Eichhorn, S.J. (2021). Postsynthesis self-and coassembly of enzymatically produced fluorinated cellodextrins and cellulose nanocrystals. Langmuir *37*, 9215–9221. https://doi.org/10.1021/acs.langmuir.1c01389.

18. Pei, Y., Wang, L., Tang, K., and Kaplan, D.L. (2021). Biopolymer Nanoscale Assemblies as Building Blocks for New Materials: A Review. Adv. Funct. Mater. *31*, 2008552. https://doi.org/10.1002/adfm.202008552.

19. Lee, J.W., Deng, F., Yeomans, W.G., Allen, A.L., Gross, R.A., and Kaplan, D.L. (2001). Direct Incorporation of Glucosamine andN-Acetylglucosamine into Exopolymers by *Gluconacetobacter xylinus* (=*Acetobacter xylinum*) ATCC 10245: Production of Chitosan-Cellulose and Chitin-Cellulose Exopolymers. Appl. Environ. Microbiol. *67*, 3970–3975. https://doi.org/10.1128/AEM.67.9.3970-3975.2001.

20. Natalio, F. (2019). Future Perspectives on Biological Fabrication and Material Farming. Small Methods *3*, 1800136. https://doi.org/10.1002/smtd.201800136.

21. Natalio, F., Fuchs, R., Cohen, S.R., Leitus, G., Fritz-Popovski, G., Paris, O., Kappl, M., and Butt, H.-J. (2017). Biological fabrication of cellulose fibers with tailored properties. Science *357*, 1118–1122. https://doi.org/10.1126/science.aan5830.

22. Rodríguez-Pérez, T., Lavandera, I., Fernández, S., Sanghvi, Y.S., Ferrero, M., and Gotor, V. (2007). Novel and Efficient Chemoenzymatic Synthesis of D-Glucose 6-Phosphate and Molecular Modeling Studies on the Selective Biocatalysis. Eur. J. Org Chem. *2007*, 2769–2778. https://doi.org/10.1002/ejoc.200700017.

23. Withers, S.G., Percival, M., and Street, I.P. (1989). The synthesis and hydrolysis of a series of deoxy- and deoxyfluoro-α-d-"glucopyranosyl" phosphates. Carbohydr. Res. *187*, 43–66. https://doi.org/10.1016/0008-6215(89)80055-2.

24. Beswick, L., Ahmadipour, S., Hofman, G.-J., Wootton, H., Dimitriou, E., Reynisson, J., Field, R.A., Linclau, B., and Miller, G.J. (2020). Exploring anomeric glycosylation of phosphoric acid: Optimisation and scope for non-native substrates. Carbohydr. Res. *488*, 107896. https://doi.org/10.1016/j.carres.2019.107896.

25. Kondo, T., and Sawatari, C. (1996). A Fourier transform infra-red spectroscopic analysis of the character of hydrogen bonds in amorphous cellulose. Polymer *37*, 393–399. https://doi.org/10.1016/0032-3861(96)82908-9.

26. Maréchal, Y., and Chanzy, H. (2000). The hydrogen bond network in I-beta cellulose as observed by infrared spectrometry. J. Mol. Struct. *523*, 183–196. https://doi.org/10.1016/S0022-2860(99)00389-0.

27. Oh, S.Y., Yoo, D.I., Shin, Y., Kim, H.C., Kim, H.Y., Chung, Y.S., Park, W.H., and Youk, J.H. (2005). Crystalline structure analysis of cellulose treated with sodium hydroxide and carbon dioxide by means of X-ray diffraction and FTIR spectroscopy. Carbohydr. Res. *340*, 2376–2391. https://doi.org/10.1016/j.carres.2005.08.007.

28. Oh, S.Y., Yoo, D.I., Shin, Y., and Seo, G. (2005). FTIR analysis of cellulose treated with sodium hydroxide and carbon dioxide. Carbohydr. Res. *340*, 417–428. https://doi.org/10.1016/j.carres.2004.11.027.

29. Wada, M., Chanzy, H., Nishiyama, Y., and Langan, P. (2004). Cellulose IIII crystal structure

and hydrogen bonding by synchrotron X-ray and neutron fiber diffraction. Macromolecules *37*, 8548–8555. https://doi.org/10.1021/ma0485585.

30. Sugiyama, J., Harada, H., and Saiki, H. (1987). Crystalline morphology of Valonia macrophysa cellulose IIII revealed by direct lattice imaging. Int. J. Biol. Macromol. *9*, 122–130. https://doi.org/10.1016/0141-8130(87)90039-0.

31. Shamshoum, M., Kuperman, O.A., Shadmi, S.K., Itkin, M., Malitsky, S., and Natalio, F. (2023). 2-NBDG Uptake in *Gossypium hirsutum* in vitro ovules: exploring tissue-specific accumulation and its impact on hexokinase-mediated glycolysis regulation. Front. Plant Sci. *14*, 1242150. https://doi.org/10.3389/fpls.2023.1242150.

32. Anastas, P., and Eghbali, N. (2010). Green chemistry: principles and practice. Chem. Soc. Rev. *39*, 301–312. https://doi.org/10.1039/B918763B.

33. Beasley, C.A. (1973). Hormonal regulation of growth in unfertilized cotton ovules. Science *179*, 1003–1005. https://doi.org/10.1126/science.179.4077.1003.

34. Beasley, C.A., and Ting, I.P. (1974). Effects of plant growth substances on in vitro fiber development from unfertilized cotton ovules. Am. J. Bot. *61*, 188–194. https://doi.org/10.2307/2441189.

35. Li, X., Liu, W., Ren, Z., Wang, X., Liu, J., Yang, Z., Zhao, J., Pei, X., Liu, Y., He, K., et al. (2022). Glucose regulates cotton fiber elongation by interacting with brassinosteroid. J. Exp. Bot. *73*, 711–726. https://doi.org/10.1093/jxb/erab451.

36. Love, J., Selker, R., Marsman, M., Jamil, T., Dropmann, D., Verhagen, J., Ly, A., Gronau, Q.F., Smíra, M., Epskamp, S., et al. (2019). JASP: Graphical statistical software for common statistical designs. J. Stat. Software *88*, 1–17. https://doi.org/10.18637/jss.v088.i02.

37. V Pereira, R., E Gallina, T., A Pereira-da-Silva, M., Kênia, S.F., and J de Menezes, A. (2021). Electrochemical Behavior of Cellulose Nanofibrils Functionalized with Dicyanovinyl Groups. In Nanofibers, *Ch. 7*, K. Brajesh, ed (IntechOpen). https://doi.org/10.5772/intechopen.96181.

38. Vaca-Garcia, C., Borredon, M.E., and Gaseta, A. (2001). Determination of the degree of substitution (DS) of mixed cellulose esters by elemental analysis. Cellulose *8*, 225–231. https://doi.org/10.1023/A:1013133921626.

39. French, A.D. (2014). Idealized powder diffraction patterns for cellulose polymorphs. Cellulose *21*, 885–896. https://doi.org/10.1007/s10570-013-0030-4.

40. Macrae, C.F., Sovago, I., Cottrell, S.J., Galek, P.T.A., McCabe, P., Pidcock, E., Platings, M., Shields, G.P., Stevens, J.S., Towler, M., and Wood, P.A. (2020). Mercury 4.0: From visualization to analysis, design and prediction. J. Appl. Crystallogr. *53*, 226–235. https://doi.org/10.1107/S1600576719014092.

41. Segal, L., Creely, J., Jr., Martin, A., and Conrad, C.M. (1959). An empirical method for estimating the degree of crystallinity of native cellulose using the X-ray diffractometer. Textil. Res. J. *29*, 786–794. https://doi.org/10.1177/004051755902901003.

42. Schindelin, J., Arganda-Carreras, I., Frise, E., Kaynig, V., Longair, M., Pietzsch, T., Preibisch, S., Rueden, C., Saalfeld, S., Schmid, B., et al. (2012). Fiji: an open-source platform for biological-image analysis. Nat. Methods *9*, 676–682. https://doi.org/10.1038/nmeth.2019.

43. Zhang, Z., Zhou, Y., Zhu, X., Fei, L., Huang, H., and Wang, Y. (2020). Applications of ESEM on Materials Science: Recent Updates and a Look Forward. Small Methods *4*, 1900588. https://doi.org/10.1002/smtd.201900588.

44. Muscariello, L., Rosso, F., Marino, G., Giordano, A., Barbarisi, M., Cafiero, G., and Barbarisi, A. (2005). A critical overview of ESEM applications in the biological field. J. Cell. Physiol. *205*, 328–334. https://doi.org/10.1002/jcp.20444.